Nanotechnology

PURPOSE-LED PUBLISHING™

PAPER

Soft-hard magnetic phase tuning of FeCo nanowire arrays by electrodeposition current density

To cite this article: Seyed Javad Hosseini *et al* 2025 *Nanotechnology* **36** 235702

IOP Publishing Nanotechnology

Nanotechnology **36** (2025) 235702 (11pp) https://doi.org/10.1088/1361-6528/add940

Soft-hard magnetic phase tuning of FeCo nanowire arrays by electrodeposition current density

Seyed Javad Hosseini[1], **Mohammad Almasi Kashi**[1,2,*] **and Amir H Montazer**[3]

[1] Department of Physics, University of Kashan, Kashan 87317–51167, Iran
[2] Institute of Nanoscience and Nanotechnology, University of Kashan, Kashan 87317–51167, Iran
[3] Department of Medical Equipment Technology Engineering, Al-Hadba University, Mosul, Iraq

E-mail: almac@kashanu.ac.ir

Received 4 February 2025, revised 10 May 2025
Accepted for publication 15 May 2025
Published 27 May 2025

Abstract

A better understanding of magnetic phases and interactions in nanomaterials can provide new pathways for the development of tunable magnetic storage media, facilitating their design and integration in nanodevices. Here, we use a pulse electrochemical method, and change the electrodeposition current density (J_{ed}) in the range of 12.50–37.50 mA cm^{-2} in order to fabricate FeCo nanowire arrays (NWAs) in mild-anodized aluminum oxide membranes. While the length and composition of the NWs are not considerably affected with increasing J_{ed}, we observe obvious changes in the shape of magnetic hysteresis curves, arising from the coupling of soft-hard phases. By investigating the crystalline properties of the NWAs, the hard phase is attributed to almost $Fe_{50}Co_{50}$ alloy structure, whereas the soft phase is due to the presence of magnetic oxides, including CoO and FeO. We obtain first-order reversal diagrams to study the two phases in more detail, indicating the involvement of interference and complex features. The increasing trends observed in hysteresis curve coercivity and squareness from 416 to 1752 Oe and 0.12–0.80 with increasing J_{ed} from 12.50 to 37.50 mA cm^{-2}, respectively, are accompanied with significant reductions in soft phase intensity and interphase magnetic interactions. Our results indicate the possibility of tuning soft-hard magnetic phases in FeCo NWAs through controlling J_{ed} during the electrodeposition process in the membranes.

Keywords: FeCo nanowire arrays, electrodeposition current density, soft phase, hard phase, magnetic oxide phase, magnetic interactions

1. Introduction

The research of materials science at the nanoscale has become important and popular in order to make technological innovations and address today's needs [1–5]. It also offers advanced nanomaterials such as nanoparticles, nanowires (NWs) and nanotubes for a wide variety of applications with potentials to be used in fundamental research and future technologies, including electronics, bioengineering, optics, and magnetism [6–8]. Among the nanomaterials, metal alloy NW arrays (NWAs) can demonstrate strong and subtle dependence of electrical, optical and magnetic properties on their structural and magnetic characteristics, which can offer tunability of a variety of device components in batteries, racetrack memories, magnetoresistive recording heads, and high density magnetic storage media [9–12].

The fabrication of rare earth-free magnetic alloy NWAs such as FeNi, FeCo, CoNi etc [13–17]. can be achieved by various techniques, including chemical (e.g., hydrothermal and sol–gel) [18–20], physical (e.g. lithography and sputtering) [16, 21] or physiochemical (e.g.

---

[*] Author to whom any correspondence should be addressed.

electrochemical deposition) [22–24] techniques. Among them, the electrochemical deposition (or electrodeposition) with adjustable voltage pulses in aluminum oxide membranes (AOMs) can cost-effectively and simply control the nucleation and growth processes, enabling us to fabricate NWAs with high aspect ratios (>10) in nanopores [9, 25, 26]. The pulse electrodeposition parameters include waveform, frequency, reduction/oxidation voltage, reduction/oxidation time, current density (J_{ed}), and off-time (T_{off}) between pulses [27–30]. By changing these parameters, structural and magnetic properties of the NWAs can be affected significantly. For example, Yu *et al* [31] fabricated Ni NWAs by varying J_{ed} between 1.2–2.5 mA cm^{-2}, influencing their crystalline and growth orientation. In this case, the crystal structure of the NWAs was transformed from polycrystalline to single crystalline with increasing J_{ed}, being accompanied with an increase in both parallel coercivity (H_{c}) and squareness (S_{q}) values. In another study, J_{ed} was found to be a determinant parameter in the growth process and crystallinity of Fe NWAs [32]. Nevertheless, by going through the literature, no attention has been paid to study the effect of J_{ed} on structural and magnetic properties of FeCo NWAs.

In this study, we fabricate FeCo NWAs using a pulse electrodeposition technique in AOMs, enabling us to change J_{ed} between 12.50 and 37.50 mA cm^{-2}. We investigate morphological, compositional and structural properties of the NWAs by different techniques. Alternatively, we study magnetic properties by employing hysteresis curve measurements and first-order reversal curve (FORC) analysis. These magnetic investigations reveal the determinant role of J_{ed} in the formation of interacting soft-hard phases with complex features in the FeCo NWAs.

2. Experimental method

2.1. AOM's fabrication process

We prepared AOMs with highly ordered honeycomb porous structure using the well-known two-step mild anodization process, as described in the literature [33, 34]. In this respect, we initially ultrasonicated Al disk samples with high purity (99.999%) in aceton for 4 min, followed by electropolishing them at a current density of 100 mA cm^{-2} using a mixture of cooled ethanol and perchloric acid (4:1 in volume) for 5 min. We performed the first step of the anodization process during 5 h by anodizing the Al disk sample using 0.3 M oxalic acid under a voltage of 40 V at a temperature of 17 °C. We etched the Al oxide layer formed in the first step of anodization using a mixed solution of 0.5 M phosphoric acid and 0.2 M chromic acid at 60 °C during 10 h. Next, we carried out the second step of anodization using the same conditions as those of the first step, except that the duration was 3 h. The second step led to the formation of an AOM with highly ordered pores, having a diameter of approximately 35 nm and an inter-pore spacing of 105 nm [32]. The Al barrier layer thickness was thinned after performing the second anodization step in order to facilitate the subsequent electrodeposition process [34]. In this case, we gradually decreased the anodization voltage from 40 to 10 V using 0.3 M oxalic acid at 17 °C, as described elsewhere [35].

2.2. Pulse electrodeposition process of FeCo NWAs

We employed an alternating current pulse electrodeposition technique [36] in order to fabricate FeCo NWAs in the previously prepared AOMs. The electrochemical cell used to fabricate the NWAs included an Al substrate (acting as the cathode electrode) and a graphite rod (as the anode electrode), while also containing 0.15 M of both $FeSO_4.7H_2O$ and $CoSO_4.7H_2O$. We also added 45 and 1 g l^{-1} of boric and ascorbic acids to the cell, respectively. The pH of the solution was set to 5.25 at 30 °C using sodium bicarbonate.

To perform the electrodeposition process, the pulse parameters consisted of a sine waveform with reduction voltage/time of 12/2.4 ms, oxidation voltage/time of 10/2.4 ms, and T_{off} of 48 ms [9, 35, 37]. It should be noted that the electrodeposition charge of all samples was set to 1 C. Meanwhile, we studied the effect of J_{ed} on the microstructure and magnetic properties of FeCo NWAs by precisely changing the current density pulse peak in the range of 12.50–37.50 mA cm^{-2} using a pulse electrodeposition system (MDK, Iran).

2.3. Instrumentation

To investigate morphological properties of the FeCo NWAs embedded in the membranes, we utilized field-emission scanning electron microscopy (FESEM, MIRA3 TESCAN) in the backscattered mode. The composition of each NWA sample was also investigated using energy-dispersive x-ray spectroscopy (EDS). We also removed the Al substrate of the samples in $CuCl_2$ solution prior to studying their crystal structure using x-ray diffraction (XRD, Philips X'Pert Pro, $\lambda = 0.154$ nm). On the other hand, we carried out high-resolution transmission electron microscopy (HRTEM, Tecnai G2 F20 Series) together with selected area electron diffraction (SAED) in order to further study the crystal structure and phases formed in the NWAs. In this regard, the sample was immersed in 0.3 M NaOH at room temperature in order to release the NWs from the membrane.

We studied room-temperature magnetic properties using vibrating sample magnetometry (VSM, MDK, Iran) with FORC capability. The VSM software enabled us to accurately set the magnetic field intensity (H) and reversal field (H_{r}) step to obtain parallel hysteresis curves and FORC diagrams [38–40] of the NWA samples. In this respect, a strong H value was applied to the sample and it was then reduced to H_{r}. In the meantime, magnetization M (H, H_{r}) was measured, resulting in FORCs. The FORC distribution ρ (H, H_{r}) was acquired as follows [41, 42]:

$$\rho_{(H,H_{\mathrm{r}})=-\frac{1}{2}\frac{\partial^2 M_{(H,H_{\mathrm{r}})}}{\partial H \partial H_{\mathrm{r}}}}. \tag{1}$$

The FORC diagram was plotted with blue and red colors as the minimum and maximum of ρ, respectively. The coordinates in the FORC diagram were also changed to the coercive field (H_{c}) and interaction field (H_{u}) axes, as given below [43]:

$$H_{\mathrm{c}} = \frac{H - H_{\mathrm{r}}}{2}, H_{\mathrm{u}} = \frac{H + H_{\mathrm{r}}}{2}. \tag{2}$$

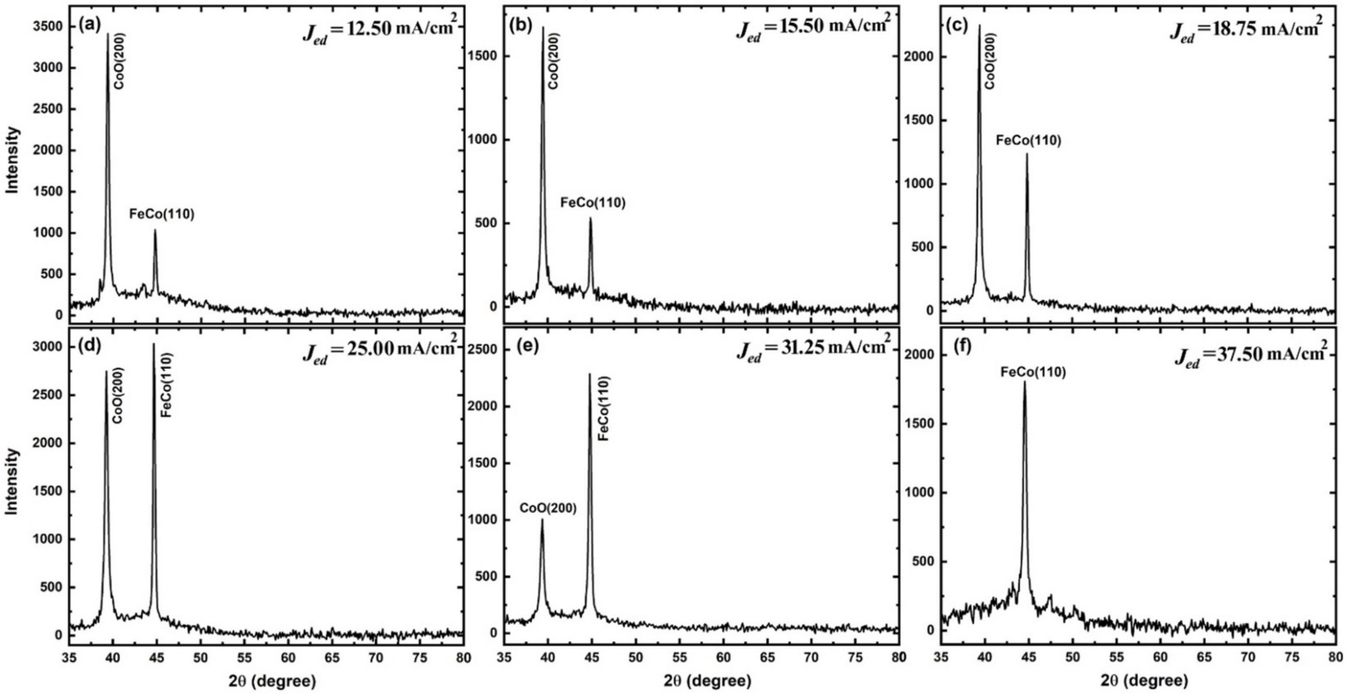

Figure 1. XRD patterns of FeCo NWAs fabricated using different J_{ed} values: (a) 12.50, (b) 15.50, (c) 18.75, (d) 25.00, (e) 31.25, and (f) 37.50 mA cm^{-2}.

3. Results and discussion

3.1. Structural results

Figures 1(a)–(f) shows XRD patterns of FeCo NWAs fabricated using different J_{ed} values (12.50–37.50 mA cm^{-2}). We observe two peaks at $2\theta = 39.63^\circ$ and 45.01° for $J_{\mathrm{ed}} = 12.50$ mA cm^{-2} (figure 1(a)), corresponding to *fcc* CoO (200) and *bcc* FeCo (110) planes, respectively (JCPDS card nos. 1300–42 and 1433–44). By increasing J_{ed} to 15.50 mA cm^{-2}, figure 1(b) shows that the intensity of the (110) peak increases relative to the (200) peak. Similarly, the XRD pattern of FeCo NWAs fabricated using $J_{\mathrm{ed}} = 18.75$ mA cm^{-2} shows the increased intensity of the (110) peak compared to the (200) one, according to figure 1(c). This variation behavior is observed by further increasing J_{ed}, so that the (200) peak disappears for FeCo NWAs fabricated using $J_{\mathrm{ed}} = 37.50$ mA cm^{-2} (see figures 1(d) and (e)). In other words, we can infer a competition between the formation of the *fcc* and *bcc* phases, depending on the J_{ed} value. For better clarity, table 1 presents the *bcc* FeCo/*fcc* CoO intensity ratios (I_2/I_1) obtained for the FeCo NWAs fabricated using different J_{ed}, indicating an increase from 0.30 to 2.27 with increasing J_{ed} from 12.50–31.25 mA cm^{-2}.

We further investigated the structural characteristics using HRTEM analysis assisted with SAED pattern of an individual FeCo NW fabricated using $J_{\mathrm{ed}} = 25.00$ mA cm^{-2}, according to figure 2. From figure 2(a), the fabrication of 35 ± 2 nm diameter FeCo NWs is indicated in the TEM image. As can be inferred from figures 2(b) and (c), in addition to the FeCo and CoO phases previously evidenced in the XRD patterns, the FeO phase exists in the NW, indicating the formation of the magnetic oxides during the pulse electrodeposition process. It should be noted that the alumina residue surrounding the individual FeCo NW causes the diameter to be larger in figure 2(b), along with the appearance of the weak halo in the SAED pattern (figure 2(c)).

Table 1. The comparison between the peak intensities of CoO and FeCo phases extracted from XRD analysis of FeCo NWAs fabricated using different J_{ed} values.

J_{ed} (mA cm^{-2})	CoO intensity (I_1)	FeCo intensity (I_2)	I_2/I_1
12.50	3420	1035	0.30
15.50	1722	583	0.34
18.75	2250	1240	0.55
25.00	2755	3035	1.10
31.25	1005	2285	2.27
37.50	—	1803	—

3.2. Morphological and compositional results

Figures 3(a)–(f) shows FESEM images of FeCo NWAs fabricated using different J_{ed} values (12.50–37.50 mA cm^{-2}) into the AOMs with a thickness of about 28 μm. The average length of the NWAs uniformly embedded in AOMs is calculated to be around 8 μm, regardless of the J_{ed} value.

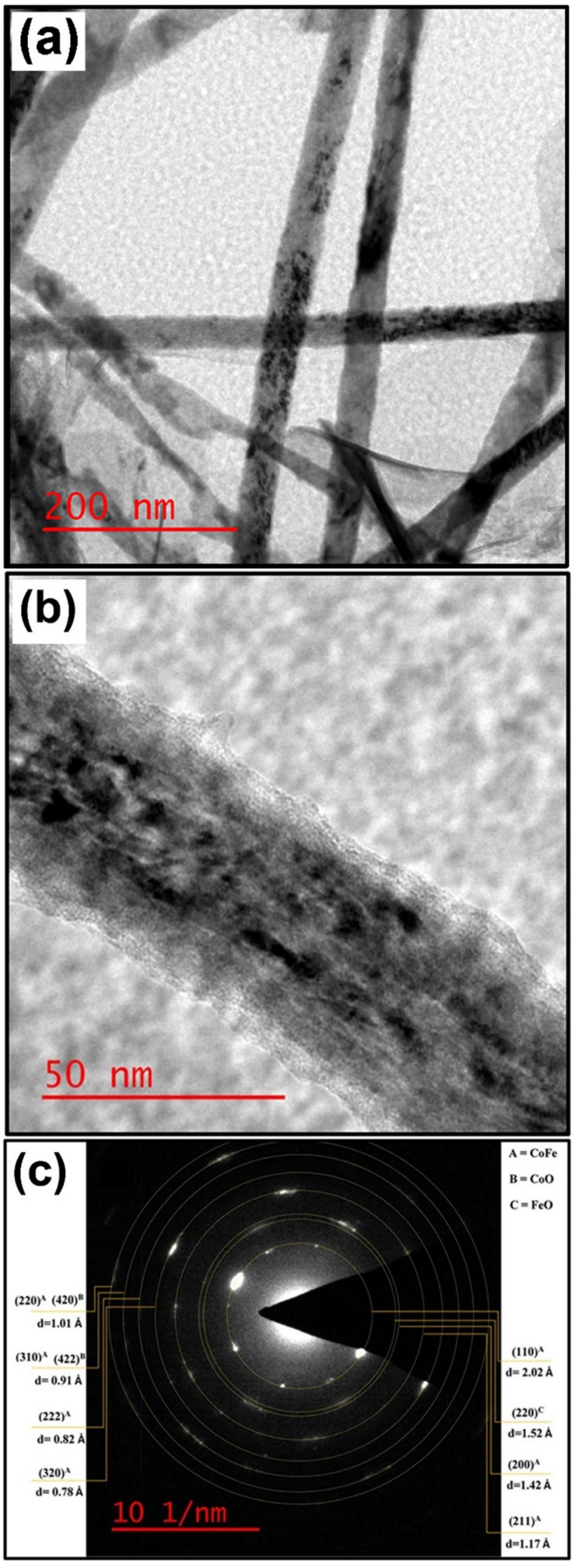

Figure 2. (a) TEM image of FeCo NWs, and (b) HRTEM image and (c) corresponding SAED pattern obtained from an individual FeCo NW. The J_{ed} used to fabricate the NWs was 25.00 mA cm^{-2}.

In other words, increasing or decreasing J_{ed} does not influence the NWA's length. Taking into account that the pore diameter of the AOM is around 35 nm, the aspect ratio of the NWAs will be very high (>280), indicating their large shape anisotropy. Higher-magnification FESEM images of the FeCo NWAs embedded in or partly detached from AOM are shown in figure 4, revealing the dendritic section (with a thickness of about 700 nm) of 35 ± 2 nm diameter NWs at the AOM's bottom, which is created due to the thinning process.

EDS spectra of FeCo NWAs fabricated using the different J_{ed} values are depicted in figures 5(a)–(f). As inferred, when $J_{ed} = 12.50$ and 15.50 mA cm^{-2}, the composition of the NWAs is almost constant to $Fe_{50}Co_{50}$. By increasing the J_{ed} above 15.50 mA cm^{-2}, the Fe content slightly increases, so that $Fe_{57}Co_{43}$ NWAs are obtained using $J_{ed} = 37.50$ mA cm^{-2}.

3.3. Magnetic results

Figures 6(a)–(f) shows room-temperature hysteresis curves of FeCo NWAs fabricated using different J_{ed} values. Noticeably, the shape of hysteresis curves changes significantly by varying J_{ed}, affecting evident magnetic parameters (e.g. H_c and S_q) and subtle magnetic characteristics such as coupling of magnetic phases and their interactions. Table 2 presents H_c and S_q values of FeCo NWAs extracted from the hysteresis curve measurements, and their variations as a function of J_{ed} are plotted in figure 7. At $J_{ed} = 12.50$ mA cm^{-2}, H_c and S_q values are found to be 416 Oe and 0.12, respectively. By increasing J_{ed} to 25.00 mA cm^{-2}, magnetic properties are enhanced by obtaining H_c and S_q values of 623 Oe and 0.27, respectively. We observe sharp increases of about 114% and 33% in the H_c and S_q values by increasing J_{ed} from 25.00 to 31.25 mA cm^{-2}. A further increase in J_{ed} to 37.5 mA cm^{-2} increases the magnetic parameters to 1752 Oe and 0.80, respectively.

From the structural results, an increasing trend of I_2/I_1 ratio was observed with increasing J_{ed}, involving the contributions of the FeCo alloy phase and the magnetic oxides. Therefore, the magnetic enhancements in the FeCo NWAs may be related to an increased amount of the hard phase (FeCo) compared to the soft phase (magnetic oxides). In this regard, the hysteresis curve shape at the maximum J_{ed} (37.5 mA cm^{-2}) shows no curvatures, likely indicating the dominance of the hard phase and/or the disappearance of the soft phase.

The FeCo NWAs fabricated using the pulse electrodeposition process outperform electrodeposited FeCo alloy thin films when it comes to the strength of magnetic anisotropy and magnetic characteristics. Notably, Zhou *et al* [44] electrodeposited FeCo alloys thin films on Ag films by varying J_{ed}. They found a decreasing trend of H_c (<22 Oe) with increasing J_{ed} to 0.0135 A cm^{-2}, which was attributed a change in the grain size. Elsewhere, Gonçalves *et al* [45] fabricated FeCo alloy thin films with different compositions using an electrodeposition method, obtaining low H_c values (<50 Oe). Therefore, FeCo alloys in the form of thin films have been found to be only soft materials, making them less appealing compared to the FeCo NWAs with soft and hard phases fabricated in the present study.

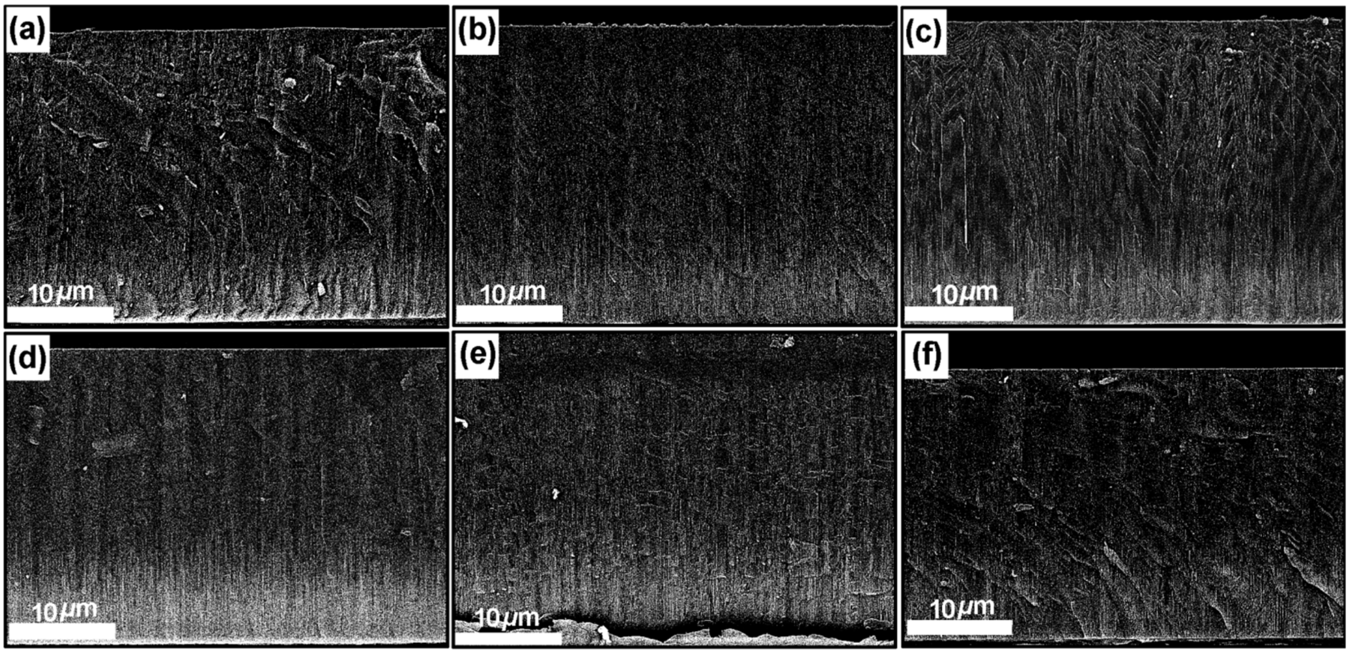

Figure 3. FESEM images of FeCo NWAs fabricated using different J_{ed} values into AOMs: (a) 12.50, (b) 15.50, (c) 18.75, (d) 25.00, (e) 31.25, and (f) 37.50 mA cm^{-2}.

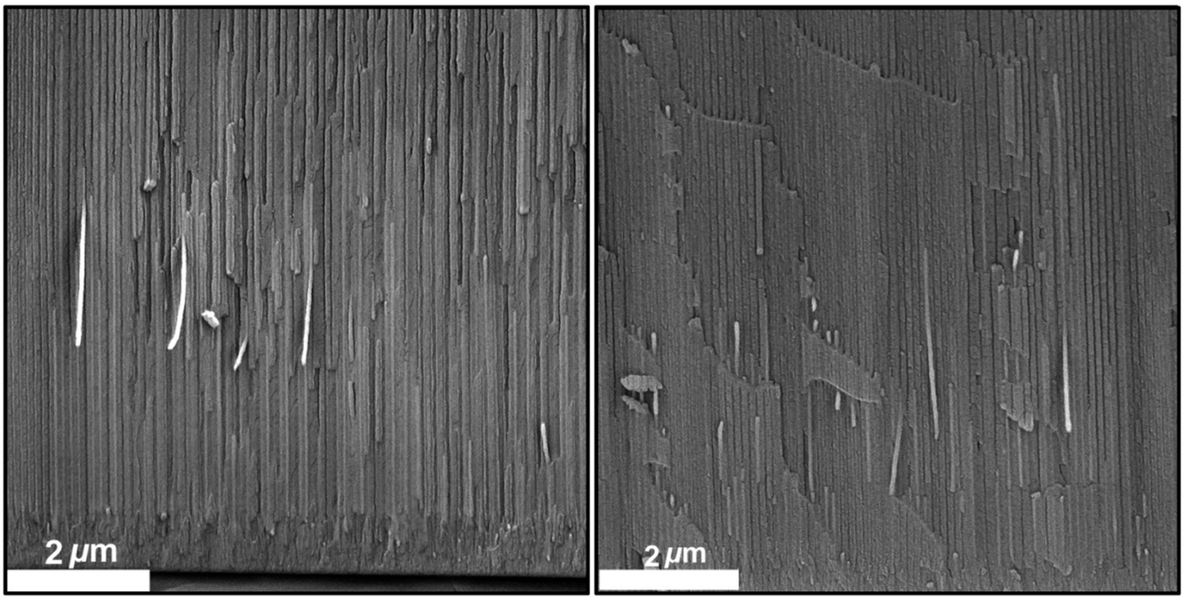

Figure 4. FESEM images of FeCo NWAs embedded in or partly detached from AOM. The J_{ed} used to fabricate the NWs was 25.00 mA cm^{-2}.

FORC diagrams were obtained from the FeCo NWAs fabricated using J_{ed} in the range of 12.50–37.50 in order to delve into the details of their magnetic phases. The results obtained are shown in figure 8. We observe in figure 8(a) that the FORC diagram of the NWAs fabricated at $J_{\text{ed}} = 12.50$ mA cm^{-2} have two noticeable distributions along the H_{c} axis. One distribution is seen around the diagram's origin, showing a FORC coercive field peak ($H_{\text{c}}{}^{\text{FORC}}$) of about 0 Oe, which can represent a soft magnetic phase.

The other distribution is less intense and located far from the origin in the range of 2500–3900 Oe with $H_{\text{c}}{}^{\text{FORC}} = 3042$ Oe, evidencing a hard magnetic phase. The

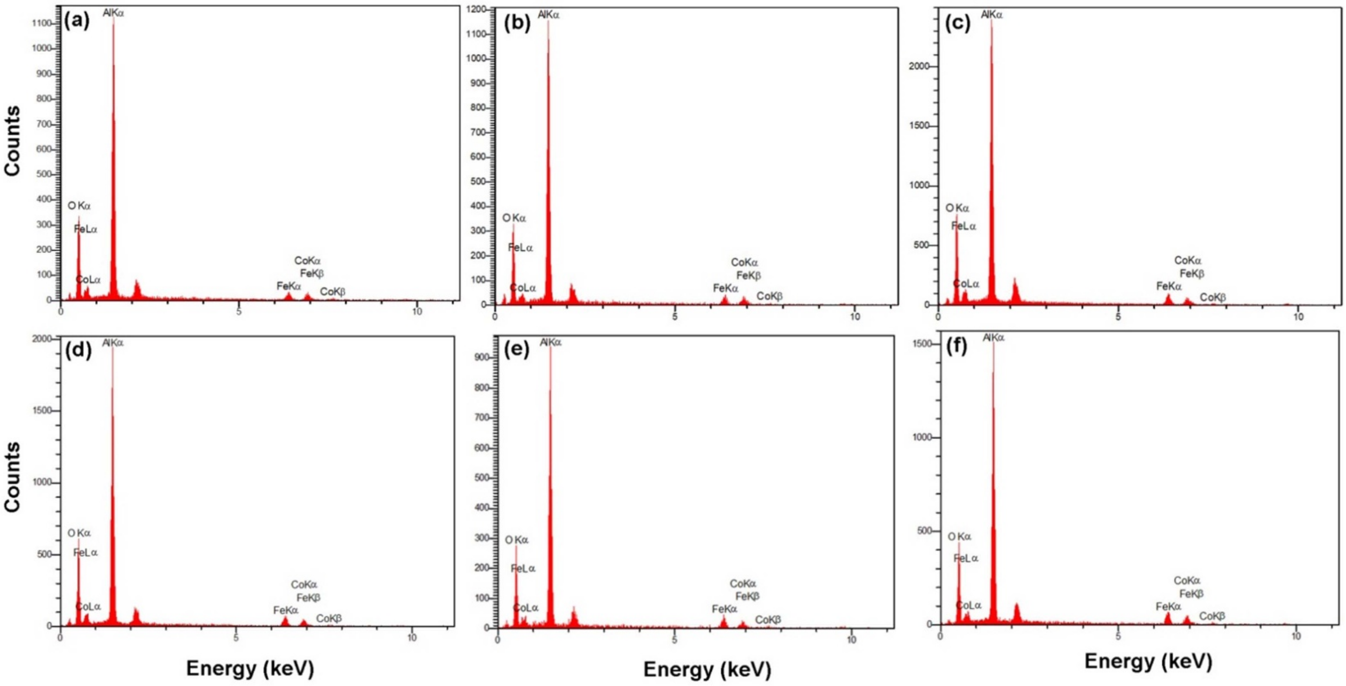

Figure 5. EDS spectra of FeCo NWAs fabricated using different J_{ed} values: (a) 12.50, (b) 15.50, (c) 18.75, (d) 25.00, (e) 31.25, and (f) 37.50 mA cm^{-2}.

overall FORC distribution is then dominated by the soft phase, leading to the significantly lower H_c value measured by the hysteresis curve (416 Oe) compared to the H_c^{FORC} of the hard phase. By increasing J_{ed} to 15.50 mA cm^{-2}, the FORC diagram (figure 8(b)) shows a wider distribution of the hard phase along the H_c axis in the range of 2000–4300 Oe, shifting the corresponding H_c^{FORC} of the hard phase to a lower value (2850 Oe), according to table 1. In addition, a pair distribution is observed in the diagram, involving positive and negative FORC peaks. This interference distribution is indicative of the coupling of soft-hard phases and their interactions, resulting in the emergence of the curvature in the corresponding hysteresis curve (see the inset of figure 6(b)). The increase in J_{ed} to 18.75 and 25.00 mA cm^{-2} has a similar effect on the FORC distribution, strengthening the magnetic phase coupling, as shown in FORC diagrams depicted in figures 8(c) and (d).

At J_{ed} = 31.25 mA cm^{-2},the intensity of the soft phase is reduced, being less localized around the origin (see figure 8(e)). Meanwhile, the distribution of the soft phase along the H_c axis increases, giving rise to a considerably stronger interference feature in the FORC diagram. This can be responsible for the sharp increase observed in the overall H_c of the hysteresis curves (from 623 to 1336 Oe) when increasing J_{ed} from 25.00 to 31.25 mA cm^{-2}. This occurrence is accompanied with the dominance of the FeCo alloy phase over the oxide phase with I_2/I_1 ratio greater than 1, according to the structural investigations presented in section 3.1. Alternatively, the FORC diagram of FeCo NWAs fabricated using J_{ed} = 37.50 mA cm^{-2} (figure 8(f)) manifests almost the disappearance of the soft phase and interference feature, leading to the maximum magnetic properties obtained by the hysteresis curve measurements. This is in agreement with the XRD pattern (figure 1(d)), in which the NWAs showed only the FeCo (110) peak. It should be noted that the broadening of the FORC distribution along the H_u axis in figure 8(f) can be related to the demagnetizing-type interactions between neighboring NWAs with dominant hard phase from the FeCo alloy.

From an applied point of view, exchange coupled media comprising both soft and hard magnetic phases have been suggested for high-density magnetic recording applications as of several years ago [46, 47]. In fact, compared to conventional magnetic recording media, the exchange coupled structure can efficiently decrease the switching field of the media without affecting its thermal stability. In this regard, it has been possible to tune the switching field of the media based on the ratio of the soft to hard phase [48, 49]. In other words, the switching field significantly decreased for a large soft/hard ratio. It is worth noting that

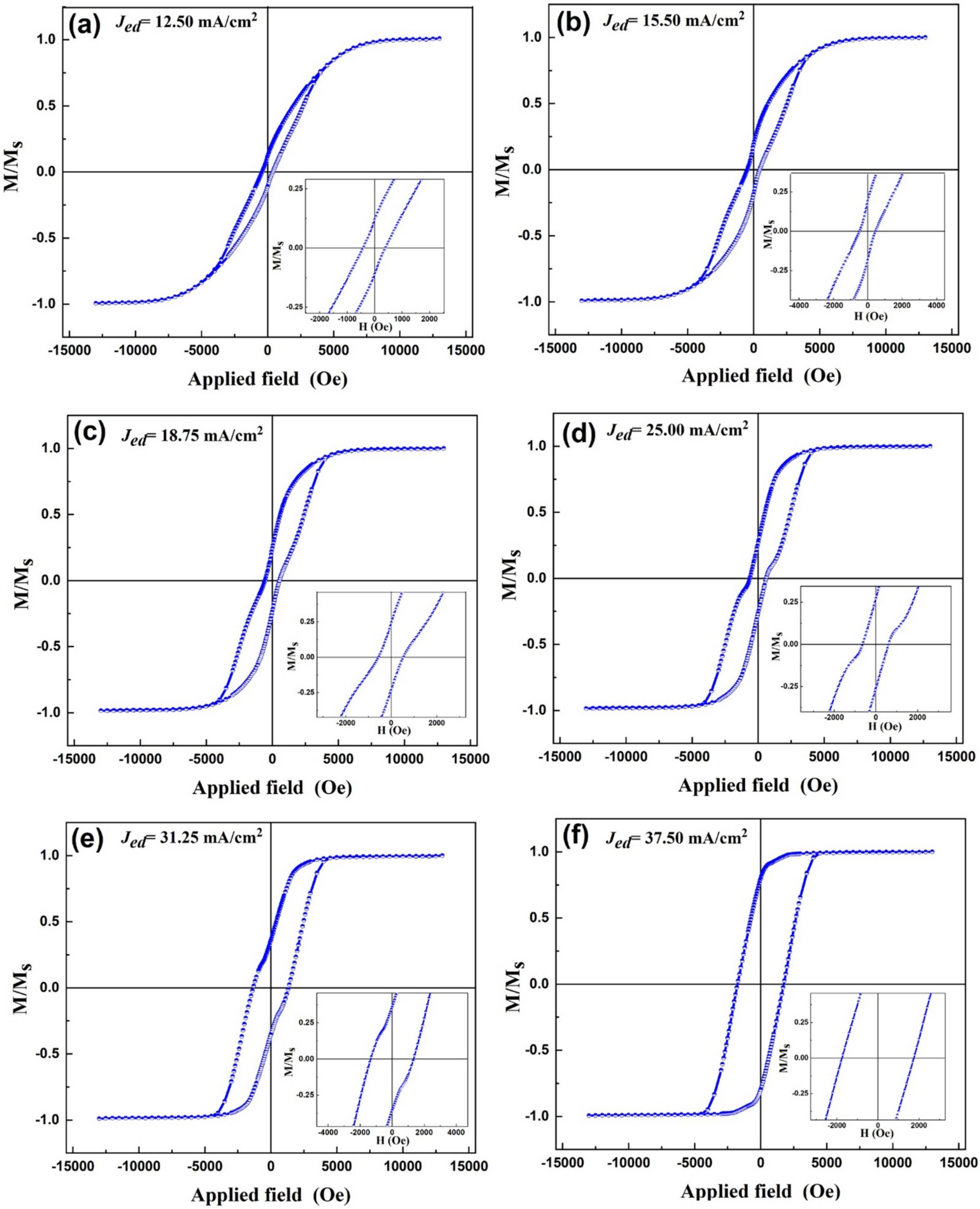

Figure 6. Room-temperature hysteresis curves of FeCo NWAs fabricated using different J_{ed} values: (a) 12.50, (b) 15.50, (c) 18.75, (d) 25.00, (e) 31.25, and (f) 37.50 mA cm^{-2}. The bottom-right insets display details of the curves around the origin.

Table 2. Magnetic parameters extracted from hysteresis curves and FORC diagrams of FeCo NWAs fabricated using different J_{ed} values.

J_{ed} (mA cm^{-2})	H_{c} (Oe)	S_{q}	$H_{\mathrm{c}}^{\mathrm{FORC}}$ (Oe)
12.50	416	0.12	3042
15.50	467	0.19	2850
18.75	551	0.24	2655
25.00	623	0.27	2453
31.25	1336	0.36	2252
37.50	1752	0.80	1798

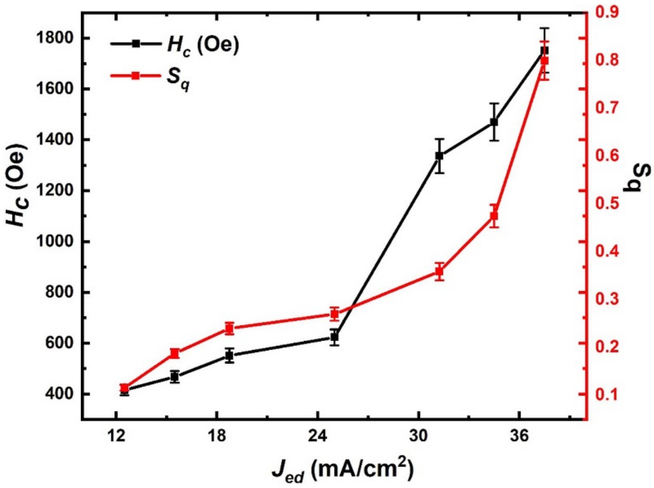

Figure 7. H_{c} and S_{q} curves as a function of J_{ed} extracted from hysteresis curve measurements of FeCo NWAs.

the amount of the soft phase should be adjusted in such a way that large magnetostatic interactions are prevented in the media, thereby achieving magnetic recording with high accuracy. Therefore, by controlling J_{ed} during the electrodeposition process, the FeCo NWAs with variable soft/ hard ratios and interphase interactions can be proposed for next-generation high-density magnetic recording or data storage applications.

4. Conclusion

We have fabricated FeCo NWAs (35 ± 2 nm in diameter and about 8 μm in length) in AOMs using different J_{ed} values (12.50–37.50 mA cm^{-2}). A competition was found between the formation of FeCo and magnetic oxide phases, depending on the J_{ed} value. In this case, the FeCo phase was continuously enhanced with increasing J_{ed}, leading to a predominant *bcc* crystal structure. The length distribution and composition of the NWAs were slightly changed with varying J_{ed}, according to FESEM and EDS analyses. Based on hysteresis curve measurements, significant increases of about 114% (from 623 to 1336 Oe) and 33% (from 0.27 to 0.36) in the H_{c} and S_{q} values were achieved by increasing J_{ed} from 25.00 to 31.25 mA cm^{-2}. FORC diagrams showed separate soft and hard phases due to the presence of the magnetic oxide and FeCo alloy phases. The interference feature representing the coupling of soft-hard phases was emerged at $J_{\mathrm{ed}} = 15.50$ mA cm^{-2} in the FORC diagram and enhanced up to $J_{\mathrm{ed}} = 31.25$ mA cm^{-2}, making its effect evident in the corresponding hysteresis curve shapes. At $J_{\mathrm{ed}} = 37.50$ mA cm^{-2}, the dominance of the hard phase caused the magnetic properties to be improved further, being in agreement with the structural results. Therefore, one can

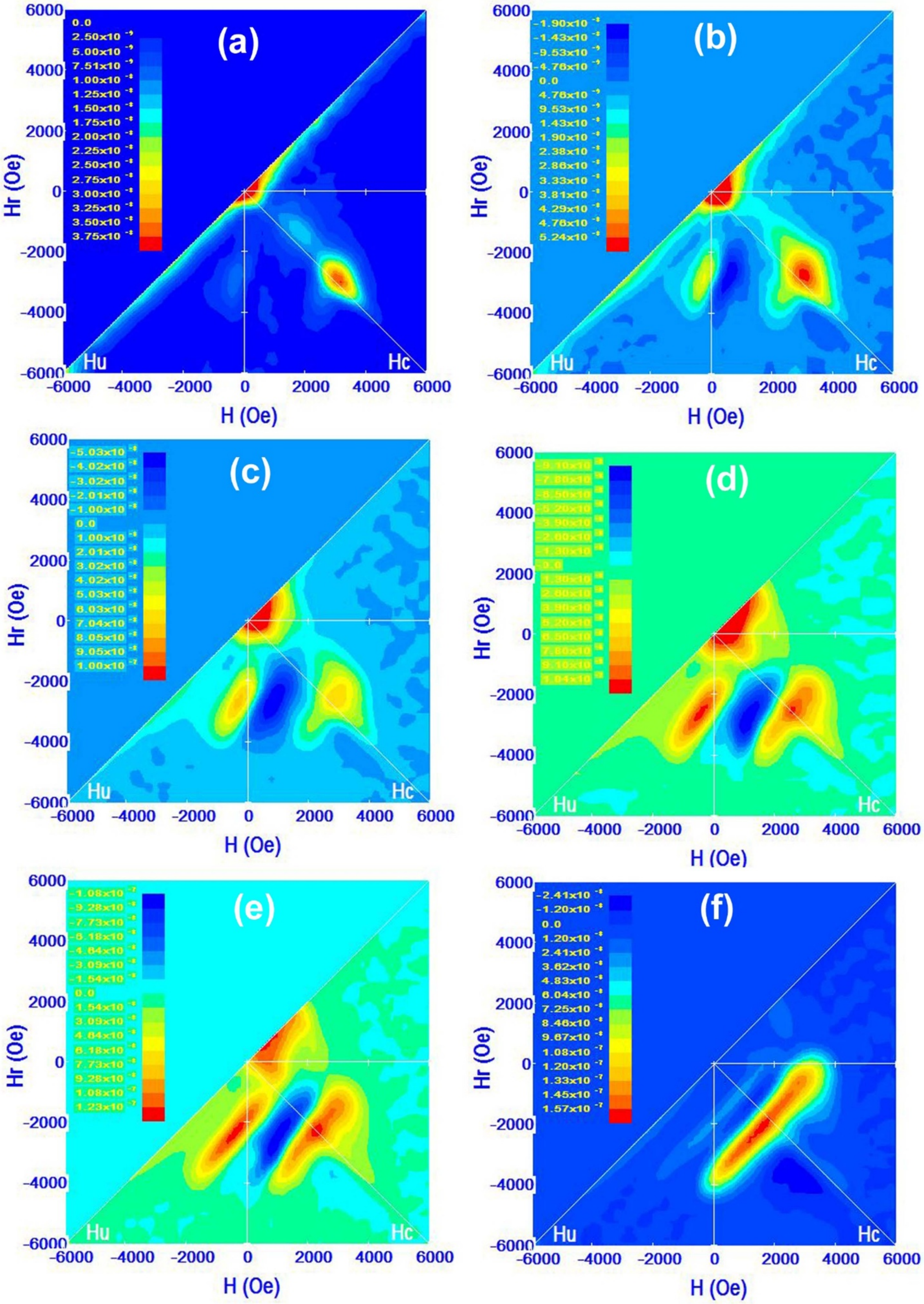

Figure 8. FORC diagrams of FeCo NWAs fabricated using different J_{ed} values: (a) 12.50, (b) 15.50, (c) 18.75, (d) 25.00, (e) 31.25, and (f) 37.50 mA cm^{-2}.

tune soft-hard magnetic phases in the FeCo NWAs through J_{ed}, offering an opportunity to maximize the performance of nanomagnet arrays for device applications.

Data availability statement

All data that support the findings of this study are included within the article (and any supplementary files).

Acknowledgments

The authors gratefully acknowledge the University of Kashan for providing the financial support of this work by Grant No. 159023/101.

ORCID iDs

Mohammad Almasi Kashi https://orcid.org/0000-0002-2742-3797
Amir H Montazer https://orcid.org/0000-0003-0629-0259

References

[1] Huang H, Feng W and Chen Y 2021 Two-dimensional biomaterials: material science, biological effect and biomedical engineering applications *Chem. Soc. Rev.* **50** 11381–485

[2] Malik S, Muhammad K and Waheed Y 2023 Nanotechnology: a revolution in modern industry *Molecules* **28** 661

[3] Chaikittisilp W, Yamauchi Y and Ariga K 2022 Material evolution with nanotechnology, nanoarchitectonics, and materials informatics: what will be the next paradigm shift in nanoporous materials? *Adv. Mater.* **34** 2107212

[4] Mohapatra J, Joshi P and Liu J P 2023 Low-dimensional hard magnetic materials *Prog. Mater. Sci.* **138** 101143

[5] El-Khawaga A M, Zidan A and Abd El-Mageed A I 2023 Preparation methods of different nanomaterials for various potential applications: a review *J. Mol. Struct.* **1281** 135148

[6] Ziegler J M, Andoni I, Choi E J, Fang L, Flores-Zuleta H, Humphrey N J, Kim D-H, Shin J, Youn H and Penner R M 2020 Sensors based upon nanowires, nanotubes, and nanoribbons: 2016–2020 *Anal. Chem.* **93** 124–66

[7] Zhu X-Y, Wang B-R, Gu Y, Zhu H, Chen L and Sun Q-Q 2021 Novel nanofluidic cells based on nanowires and nanotubes for advanced chemical and bio-sensing applications *Nanomaterials* **11** 90

[8] Sajid M and Płotka-Wasylka J 2020 Nanoparticles: synthesis, characteristics, and applications in analytical and other sciences *Microchem. J.* **154** 104623

[9] Kashi M A and Montazer A 2022 Template-based electrodeposited nonmagnetic and magnetic metal nanowire arrays as building blocks of future nanoscale applications *J. Appl. Phys.* **55** 233002

[10] Li S, Jin H and Wang Y 2023 Recent progress on the synthesis of metal alloy nanowires as electrocatalysts *Nanoscale* **15** 2488–515

[11] Moreno J A, Bran C, Vazquez M and Kosel J 2021 Cylindrical magnetic nanowires applications *IEEE Trans. Magn.* **57** 1–17

[12] Nehra M, Dilbaghi N, Marrazza G, Kaushik A, Abolhassani R, Mishra Y K, Kim K H and Kumar S 2020 1D semiconductor nanowires for energy conversion, harvesting and storage applications *Nano Energy* **76** 104991

[13] Shao Z and Ren S 2020 Rare-earth-free magnetically hard ferrous materials *Nanoscale Adv.* **2** 4341–9

[14] Mamniashvili G, Donadze G, Gegechkori T, Gavasheli T, Maisuradze A and Kelikhashvili V 2022 Study of domain wall pinning in the rare earth-free permanent magnets using nuclear magnetic resonance method *Air Transp.* **16** 25–35

[15] Wang Y, Yang Z, Li C, Wu Q, Liu W, Li Y, Cong L, Ma X, Zhang H and Lu Q 2022 Enhanced coercivity in Co nanowires via manipulation of head morphology *J. Magn. Magn. Mater.* **561** 169695

[16] Kaur D 2022 *Nanowire Magnets: Synthesis, Properties, and Applications, Fundamentals of Low Dimensional Magnets* (CRC Press) pp 41–57

[17] Wu C and Jin J 2022 *Frontiers in Magnetic Materials: From Principles to Material Design and Practical Applications* (CRC Press)

[18] Mamniashvili G, Gegechkori T, Zedginidze T, Petriashvili T, Janjalia M, Gavasheli T and Kezerashvili R Y 2024 Chemical synthesis of cobalt nanowires in an external magnetic field and their characterization by NMR *J. Appl. Spectrosc.* **91** 21–24

[19] Zeng X-L, Sivanesarajah I and Hartmann U 2023 Conversion of hard to soft magnetic ferrite nanowires by paramagnetic shielding *Solids* **4** 304–15

[20] Mukhtar A, Wu K and Cao X 2020 Magnetic nanowires in biomedical applications *Nanotechnology* **31** 433001

[21] Huang Q and Zhu Y 2021 Patterning of metal nanowire networks: methods and applications *ACS Appl. Mater. Interfaces* **13** 60736–62

[22] Ruiz-Gómez S, Fernández-González C and Perez L 2022 Electrodeposition as a tool for nanostructuring magnetic materials *Micromachines* **13** 1223

[23] Ruiz-Gómez S, Fernández-González C and Perez L 2022 s Note: MDPI stays neutral with regard to jurisdictional claims in published

[24] Vazquez M 2022 Cylindrical nanowire arrays: from advanced fabrication to static and microwave magnetic properties *J. Magn. Magn. Mater.* **543** 168634

[25] Mukhtar A and Wu K 2022 Coupled electrodeposition and magnetic properties of ternary CoFeW alloys *Mater. Charact.* **192** 112246

[26] Piraux L 2020 Magnetic nanowires *Appl. Sci.* **10** 1832

[27] Esfahani M N, Samanifar S, Ghasemi A, Rashidi A, Paimozd E and Tavoosi M 2021 Fabrication and magnetic characteristics of electrodeposited FeCr nanowire arrays *J. Magn. Magn. Mater.* **537** 168218

[28] Saadinia E, Kashi M A and Montazer A H 2024 Fabrication and magnetic properties of pulse electrodeposited FeSn nanowire arrays *J. Phys. Chem. Solids* **186** 111797

[29] Mottaghian S, Najafi M, Rafati A A and AsgharTerohid S A 2023 Structural, morphological, angular dependent of magnetic properties and FORC analysis of CoFeIn novel nanowire alloys *Mater. Sci. Eng. B* **290** 116334

[30] Paimozd E, Mirzaee O, Ghasemi A and Tajally M 2021 Structural and magnetic characterization of (FeCo)$_{1-x}$ Cr$_x$ nanowires array prepared by pulsed electrodeposition *Appl. Phys. A* **127** 1–12

[31] Yu Y, Li J, Wang J, Wu X, Yu C, Xu T, Chang B, Sun H and Arandiyan H 2019 Orientation growth and magnetic properties of electrochemical deposited nickel nanowire arrays *Catalysts* **9** 152

[32] Noori F, Kashi M A and Montazer A H 2022 Current density-induced emergence of soft and hard magnetic phases in Fe nanowire arrays *Nanotechnology* **34** 075701

[33] Patel Y, Janusas G and Palevicius A 2021 Fabrication of nanoporous free standing anodic alumina using two-step anodization for applicability in microhydraulic system as

nano filter using surface acoustics *Mater. Today* **45** 5059–64

[34] Ahmadzadeh M, Kashi M A, Noormohammadi M and Ramazani A 2021 Small-diameter magnetic and metallic nanowire arrays grown in anodic porous alumina templates anodized in selenic acid *Appl. Phys. A* **127** 450

[35] Noori F, Ramazani A and Kashi M A 2018 Controlling structural and magnetic properties in CoNi and CoNiFe nanowire arrays by fine-tuning of Fe content *J. Alloys Compd.* **756** 193–201

[36] Kashi M A, Ghaffari M and Torshizi F 2020 Structural and magnetic tunability of Co/Cu multilayer nanowires induced by electrolyte acidity and spacer layer thickness *J. Alloys Compd.* **820** 153087

[37] Samanifar S, Kashi M A, Ramazani A and Alikhani M 2015 Reversal modes in FeCoNi nanowire arrays: correlation between magnetostatic interactions and nanowires length *J. Magn. Magn. Mater.* **378** 73–83

[38] Burks E C, Gilbert D A, Murray P D, Flores C, Felter T E, Charnvanichborikarn S, Kucheyev S O, Colvin J D, Yin G and Liu K 2020 3D nanomagnetism in low density interconnected nanowire networks *Nano Lett.* **21** 716–22

[39] Alicheraghi L, Ghasemi A, Paimozd E and Nasr-Esfahani M R 2024 Insight into the intra and inter-wire magnetic interactions of Co nanowire arrays by FORC diagrams *J. Supercond. Nov. Magn.* **37** 1–9

[40] Pierrot A, Béron F and Blon T 2020 FORC signatures and switching-field distributions of dipolar coupled nanowire-based hysterons *J. Appl. Phys.* **128** 093903

[41] Abbas M, Montazer A, Alshoca Z, Ramazani A and Kashi M A 2024 Magnetic reversal mode investigation of FeCo/Cu multilayered nanowires with different Cu layer lengths *J. Supercond. Nov. Magn.* **37** 459–67

[42] Elmekawy A, Iashina E, Dubitskiy I, Sotnichuk S, Bozhev I, Napolskii K, Menzel D and Mistonov A 2020 Magnetic properties and FORC analysis of iron nanowire arrays *Mater. Today Commun.* **25** 101609

[43] Mousavi S E, Ramazani A and Kashi M A 2024 Angular first-order reversal curve analysis of FeNi/Cu multilayered nanowire arrays with different diameters *J. Magn. Magn. Mater.* **589** 171596

[44] Zhou D, Zhou M, Zhu M, Yang X and Yue M 2012 Electrodeposition and magnetic properties of FeCo alloy films *J. Appl. Phys.* **111** 07A319

[45] Gonçalves S, Andrade V, Sousa C T, Araújo J P, Belo J H and Apolinário A 2023 Tunable iron–cobalt thin films grown by electrodeposition *Magnetochemistry* **9** 161

[46] López-Ortega A, Estrader M, Salazar-Alvarez G, Roca A G and Nogués J 2015 Applications of exchange coupled bi-magnetic hard/soft and soft/hard magnetic core/shell nanoparticles *Phys. Rep.* **553** 1–32

[47] Victora R H and Shen X 2005 Exchange coupled composite media for perpendicular magnetic recording *IEEE Trans. Magn.* **41** 2828–33

[48] Victora R H and Shen X 2008 Exchange coupled composite media *Proc. IEEE* **96** 1799–809

[49] Casoli F, Nasi L, Albertini F and Lupo P 2016 Exchange-coupled Composite Media *Ultrahigh-Density Magnetic Recording—Storage Materials and Media Designs* ed G Varvaro and F Casoli (Pan Standford) p 48